JOURNAL OF AIRCRAFT
Vol. 48, No. 3, May–June 2011

Uncertainty Analysis of a Dynamic Model of a Novel Remotely Piloted Airship

William Becker* and Keith Worden†
University of Sheffield, Sheffield, England S1 3JD, United Kingdom
and
Maneula Battipede‡ and Cecilia Surace§
Politecnico di Torino, 10129 Torino, Italy

DOI: 10.2514/1.C031207

As the sophistication of finite element models increases, the need to investigate the effects of uncertainties in model inputs becomes increasingly important in the interests of developing a robust model. A novel design of an unmanned airship is under development at the Politecnico di Torino, Italy. Structural and fluid–structure interaction models were developed to ascertain the response of the structure under operational and aerodynamic loading; however, uncertainties in material properties (due to variation with temperature), pressure, and aerodynamic loading necessitated an uncertainty analysis. Since the computational expense of a large finite element model makes Monte Carlo methods impractical, a probabilistic Bayesian uncertainty analysis was performed, whereby the output of the model is sampled over a set of input points and the response of the model is emulated by a Gaussian process. Quantities pertaining to uncertainty analysis were then inferred, allowing a reliable uncertainty analysis to be performed for considerably less computational expense than conventional Monte Carlo methods. The results showed that uncertainty in model stress and deflection is indeed significant, although the highly nonlinear response of the fluid–structure interaction model required a high sampling density in order to accurately emulate its response.

I. Introduction

AIRSHIPS, a subset of lighter-than-air aircraft, have been in use in some form or another since the 18th century. Despite the obvious caveats, airships still retain certain attractive advantages, including the possibility of long flight times for a comparatively low cost, the ability to remain virtually stationary, and the ability to take off vertically. As such, there are still a number of airship projects ongoing around the world. Liao and Pasternak [1] provide a nice summary of various projects and designs in progress (albeit from 2009).

One set of applications in which airships perform particularly well compared with heavier-than-air aircraft is that of surveillance, monitoring, and communications relay. Such airships are often relatively small and unmanned, with the applications requiring lengthy flight times, yet airships are particularly well suited due to their ability to remain aloft for long periods with little cost and the stable and vibration-free platform that they can provide for delicate surveillance equipment. Furthermore, since they are practically noise free and use little fuel, they are well suited for use in environmental and oceanographic monitoring. However, there are several drawbacks in conventional designs: since airships have very large profiles, they are very susceptible to disturbance from crosswinds, a problem that is particularly undesirable in landing and takeoff. Additionally, at low velocities, the rudders and elevators that are used for maneuvering are very ineffective, since they depend on lateral air movement to generate any steering force.

This paper concerns the design of a new and innovative airship design, ongoing at the Department of Aerospace Engineering in the Politecnico di Torino in Turin, Italy [2]. The design aims to address certain problems that limit the effectiveness of classical airship designs (see later). To reduce costs in prototypes and testing, finite element (FE) models have been integral in the development of the project to date. However, as the sophistication of simulations and reliance thereon have increased in all many fields of engineering, it has become increasingly apparent that uncertainties in model inputs can have profound and unexpected effects on the outputs of interest. In the case of the airship, a great number of parameters must be input into a FE model, such as material properties, boundary conditions, and loading conditions. Any number of these can be subject to uncertainties resulting from lack of knowledge, varying operating conditions, or other reasons. As such, a series of uncertainty analyses has been performed in this paper to investigate the effects of uncertainties in loading and material properties in models created to test proposed airship designs, since design decisions are taken based on results from such models (i.e., if the model outputs are uncertain, then it is difficult to make a clear decision about the choice of design). To deal with the significant computational time required for the most comprehensive models, a Bayesian uncertainty analysis method was adopted that uses a metamodel-based approach to reduce overall computational expense.

II. Design

A. Overview

To combat the problems mentioned with conventional airship designs and expand the range of operable weather conditions, a new design has been proposed in [3] called the Elettra Twin Flyer (ETF). Figure 1 illustrates the concept of the new design. The design innovations are twofold. First, there are two gas envelopes rather than one, positioned side by side. This allows a smaller profile for the equivalent lift. The two balloons are connected by a rigid structure that also acts as a platform for affixing the payload and operational equipment. Second, the ship is moved in all six degrees of freedom by a series of directional propellers; the advantage being that the ship can be maneuvered effectively without the requirement of forward motion. This movement of the airship is controlled by a specialized control system; details can be found in [4,5]. Altogether, the innovations should give the ship greatly increased maneuverability at low velocities and allow the ETF to hover with the prow orientated in

Received 9 August 2010; revision received 3 December 2010; accepted for publication 7 December 2010.

*Ph.D. Student, Department of Mechanical Engineering, Mappin Street.
†Professor, Department of Mechanical Engineering, Mappin Street.
‡Assistant Professor, Department of Aeronautical and Space Engineering, corso Duca degli Abruzzi 24.
§Assistant Professor, Department of Structural and Geotechnical Engineering, corso Duca degli Abruzzi 24.

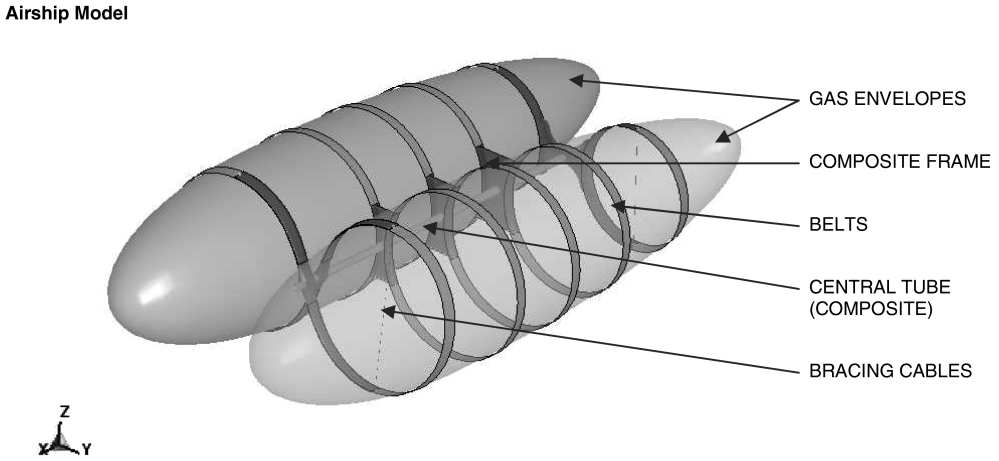

Fig. 1 Illustration and arrangement of materials in the ETF.

any direction, even in adverse weather conditions. An early, small-scale proof-of-concept design of the ETF has been designed, manufactured, and tested. In continuation of this, two separate designs are being considered for the prototype [2]; this paper concerns a continuation of the structural analysis of one of these models.

A series of previous analyses were performed to ascertain the dimensions of the structure. The thickness and shape of the structure are governed by the stresses due to loading; however, changing the structure to withstand these stresses will inevitably change the mass, which then will require a greater or lesser volume of helium for buoyancy.

This in turn will change the overall size of the airship and change the loading. The final design is therefore the result of an informal iterative process; as such, the models in this paper do not represent final designs but parts of the iteration. The models investigated here are 36 m in length, this being the length required for sufficient buoyancy to support the total weight of the structure and payload (approximately 3 tons) as calculated by previous analyses. The length is only mentioned here to give an idea of the scale of the airship, since the final design is expected to be of a similar magnitude of length.

B. Material

The two materials that comprise the majority of the airship are the envelope material and the frame material (see Fig. 1, showing material divisions in the model). Desirable material properties of the frame material include low density while being as stiff as possible, since large deformations of the structure would alter the aerodynamic response and have unwanted effects on the control system. It was concluded, after some simple preliminary simulations [6,7], that the most suitable material would be a sandwich layup consisting of layers of carbon/epoxy T300 15k/976 composite on either side of an Ultracor® honeycomb core. This configuration resulted in a quasi-isotropic material at the macroscopic level to simplify modeling.

It was found that the material properties of the composite varied significantly with change in temperature [8]. Since the airship is potentially operating in conditions of $\pm 50^{\circ}$C (depending on altitude, location, and weather), the uncertainties in material properties were expected to have a substantial effect on the response of the structure to loading. Figure 2 illustrates the variation of stiffness of the sandwich layup with varying temperature. By fitting a polynomial function to this curve, it was possible to express stiffness as a function of temperature so that temperature could be used as the uncertain input variable rather than stiffness.

The envelope material was required to possess a high tensile stiffness with minimal weight. Additionally, it should have low permeability (to helium) and be resistant to degradation from UV radiation. A number of candidate materials were under consideration, and one of these (nylon 6) was selected and tested to failure at a range of temperatures. Similar to the composite material, preliminary models suggested that the strain on the material was always within the linear region of the stress–strain curve. As such, a relationship could be established between temperature and elastic modulus (also presented in Fig. 2).

III. Modeling

The modeling of the airship was performed to reveal the stress and deformation of the airship under normal and extreme loading conditions. As mentioned, control of the structure is performed by a number of directional propellers (currently) based on the assumption that the structure is rigid. This is an important point, because even minor deformations and rotations of the arms on which the propellers are located can have effects on the control system that are hard to predict. One main objective of the FE analysis was to thus quantify deformation in certain parts of the structure under a variety of loading conditions. Furthermore, it was important to know whether the structure could withstand various loads without failure and make informed decisions regarding, for example, thicknesses and types of material.

Published literature concerning airship modeling is scarce, probably due to the small number of airship design projects in existence and the fact that the heyday of airship design was many years before the rise of computer modeling. Furthermore, the simulation of airships poses particular difficulties to the modeler, given that it involves interactions between flexible membranes and stiff structures, aerodynamic loading, and is unconstrained in all degrees of freedom. Bessert and Frederich [9] examined the effects of aeroelasticity in a classical airship design by coupling and iterating between structural and fluid solvers. Liu et al. [10] performed a similar analysis, concluding that aeroelasticity has an effect on the

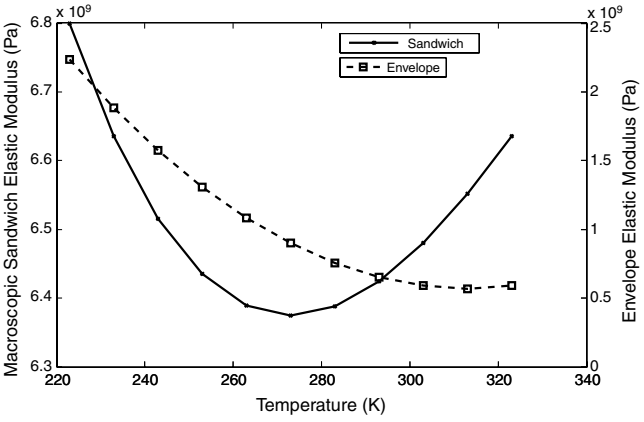

Fig. 2 Interpolated material properties of sandwich and envelope.

pressure distribution of a conventional airship balloon. Li et al. [11] performed an analytical analysis of the aerodynamics of a flexible airship. However, the authors of this paper are not aware of any consideration of uncertainties in airship modeling.

Three models were constructed. First, a preliminary linear static model investigated deformations on the structure without consideration of the presence of the membrane; this was used to estimate structural dimensions for the more sophisticated models. Next, a nonlinear model was constructed that included the membranes and investigated the uncertainties in pressure and material properties as a result of temperature. Finally, a full fluid–structure interaction (FSI) model considered the effect of gusts of wind incident at different angles to the airship. To deal with nonlinearities in the latter two models, the solution was performed in the primarily explicit-dynamic code LS-Dyna. This solver is capable of handling highly nonlinear and transient simulations and the coupling of Lagrangian and arbitrary-Lagrangian–Eulerian (ALE) meshes as required for FSI in this approach.

A. Nonlinear Dry Simulation

Figure 3 illustrates the mesh of the nonlinear dry model. Although, as previously mentioned, the material could be treated as linear, the inclusion of the gas envelopes brought a greater possibility of large deformations, which would require the use of nonlinear finite strain elements. An extra problem with the inclusion of the gas envelopes was that, in flight, they are in a prestressed state. To determine this state before further simulation, it was necessary to inflate the membranes, that is, to estimate the uninflated size and apply a pressure so that the balloons expanded into the frame. On contact between balloon and frame nodes, coupling occurred to unify the structure.

Loading on the structure was the same as the linear simulation, with the addition of the helium pressure on the membranes. Additionally, buoyancy was considered. Given that buoyancy is not uniform along the length of the airship, each balloon volume was considered as 20 discrete volumes, on the upper surfaces of which the buoyancy was applied as a set of nodal forces, the magnitude being a function of the volume of underlying helium. The advantage of this over the static simulation was that it gave a much more accurate distribution of pressure over the frame, which was previously only estimated. Since inertia relief is not available in nonlinear simulations, the simulation was performed using an explicit-dynamic solver so that rigid body motion was allowed to occur. This more accurately reflects the true nature of the problem, because airships are of course unconstrained when in flight and displacements and stresses vary as a function of time.

B. Nonlinear Wet Simulation

One further problem of concern was to understand how the airship would respond under aerodynamic loading, which was hitherto neglected in modeling. The forms and magnitudes of aerodynamic loading can vary greatly, from the response of the structure in steady-state flow to ramped or stepped loading (i.e., from gusts of wind in still air). The gust is an important aspect in the study of the interaction of any aircraft with the real atmosphere. It must be taken into consideration for two reasons: first, to consider the dynamic response of the aircraft, and second, to evaluate the implications of the gust on the stresses in the structure. With regard to the latter, the most critical situation is the vertical gust. However, in the case of the ETF, operational velocity is low, and an important design objective is the ability to hover in adverse weather conditions. In this case, therefore, the horizontal gust becomes of interest.

The form of gust used is the classic constant-gradient gust referred to, for example, in the European Aviation Safety Agency regulations [12]. The velocity profile of the linear gust is known to closely follow that of a natural gust; therefore, it was thought to be reasonable to use this slight simplification, given that in the structural analysis, the model nonlinearities are of much greater importance.

Since the pressure distribution on a nontrivial structure due to a particular gust of wind is far from obvious (especially at certain angles), a FSI model was created, whereby an ALE mesh was overlapped with the Lagrangian mesh used for the dry model. The possibility of structural deformation that would change the boundary conditions of a standard computational fluid dynamics model necessitates this approach. The ALE mesh combines the benefits of the Lagrangian and Eulerian mesh approaches, respectively, that the mesh is allowed to move in space (thus limiting the size of the mesh necessary) and that the material can flow through the mesh, allowing the very large deformations that are characteristic in fluid flow. An extensive discussion on the ALE method is found in [13]. The two meshes are coupled together using a penalty-based approach in the explicit solver so that they iteratively interact with each other [14]. Figure 4 illustrates the arrangement of the two meshes. The ALE mesh is cylindrical, because it allows investigation of different incident gust angles, as the airship could simply be rotated in the mesh without the need for extra preprocessing.

The ALE mesh is of a multimaterial type that allows mixing of different materials in individual elements. It was configured so that it was filled with stationary air surrounding the airship; then, at the edge nodes of the mesh on one side (the inlet to the mesh), the air was constrained to move at 10 m/s in the direction of the ship. The ship mesh was orientated at an angle μ from the direction of the gust. This closely simulates the effect of a sudden gust of air hitting the airship hovering in stationary air. A key advantage of the ALE mesh formulation is that it can be tied to the airship mesh so that when the airship moves as a result of the gust impact, the mesh moves with the structure, which means that a smaller mesh can be used even if the airship is displaced by a significant amount.

The air is defined by a constitutive model, which gives the deviatoric stresses (not considering possible changes in volume), and

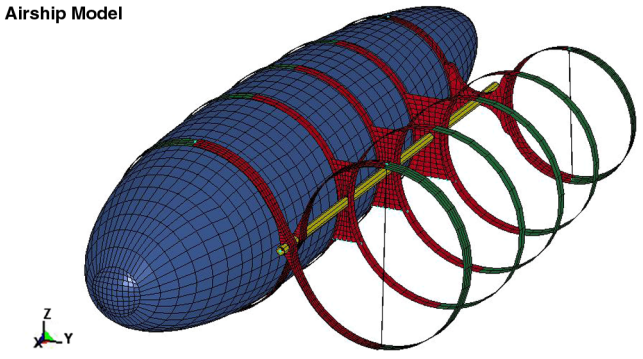

Fig. 3 Mesh of nonlinear dry simulation (one balloon removed for clarity).

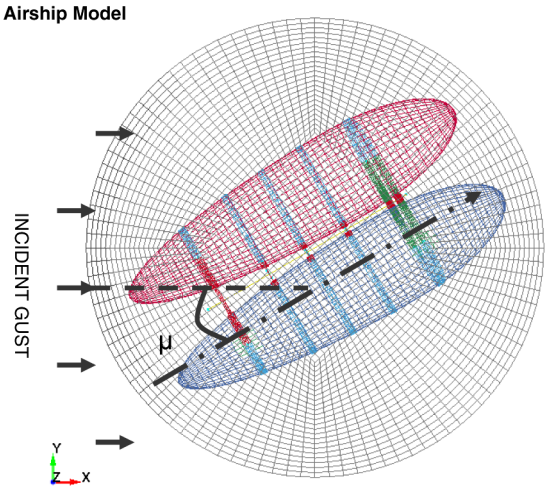

Fig. 4 Illustration of cylindrical ALE mesh overlapping Lagrangian airship mesh, viewed from above; μ = angle between gust direction and ship axis.

an equation of state, which provides the pressure component. This allows modeling of compressible, viscous flow, although without consideration of turbulence, representing a first approximation of the airflow around the structure for use in uncertainty analysis.

Although there are many conceivable uncertainties associated with the definition of the gust hitting the airship, in this analysis, only the wind angle was investigated. After adding the fluid mesh, the run time of the model became very substantial due to the large extra number of ALE elements, which also require extra processing for the advection steps (the operation of translating the ALE nodes). As such, for this stage of the investigation, the other uncertainties were treated as known to save on analysis time, although they may be investigated in future analyses.

IV. Uncertainty Analysis

Uncertainties have become of increasing concern in recent years. Modern computer codes can simulate highly complex physical events, yet the more complex the model, the more information must be input in the definition of the simulation. Often, at least some of these parameters are not known exactly; material properties, for example, vary as a function of temperature, so how does one decide at which temperature to test a model? The problem is the same in loading; often, the forces or pressures on a model could be anywhere within a wide range. Other parameters may simply not be known exactly because of a lack of complete knowledge.

One approach to solving this problem is to investigate the model at extremes in the input parameter space, for example, at the maximum and minimum temperatures (it is assumed that at least a plausible range of a given input parameter is known). However, if the response of the model is nonlinear with respect to any of the input parameters, there is no guarantee that a maximum or minimum output value will be observed at the maximum or minimum of the input. A more trustworthy approach would then be to run the model at many different points over the input space, giving a clearer idea of the response of the model. This is known as global uncertainty analysis: globally investigating the output uncertainty in a model due to uncertainty in its inputs. A furtherance of uncertainty analysis is sensitivity analysis, which seeks to understand and quantify how output uncertainty is affected by particular inputs; Saltelli et al. provide a description of the most widely used methods [15].

A key requirement in uncertainty and sensitivity analysis is to somehow quantify the input uncertainties. Although there are many ways of doing this (see [16] for an excellent summary), a well-established approach is to define probability distributions for each input parameter. Ideally, then, a joint distribution $P(\boldsymbol{x})$ (where $\boldsymbol{x}$ is the vector of d input variables) can be formed. In this probabilistic sense, the propagation problem is then to find the unknown probability distribution of any output quantity of the model. Monte Carlo (MC) methods can provide this; however, the number of model runs required to accurately estimate the distribution becomes prohibitively high for complex models with more than a small number of uncertain inputs; in other words, it would simply take too long.

One way to combat this problem is to use an emulator-based approach. The idea is that the model is treated as a mathematical function (which, of course, it is), but it is generally of such complexity to be completely intractable for analytical uncertainty analysis. However, in many cases, the model can itself be modeled by a much simpler emulator that is considerably cheaper to run. The problem then reduces to fitting a suitable emulator to the model using a set of training data and analyzing the emulator to draw meaningful estimates pertaining to uncertainty and sensitivity analyses. A simple example of this would be to fit a polynomial function; however, this is of limited flexibility since it forces an assumption about the order of the function. An alternative approach is outlined here that follows that described by Oakley and O'Hagan [17].

A. Gaussian Process Regression

One suitable emulator for modeling computer codes, first introduced in this context by Sacks et al., is based on a powerful regression paradigm from machine learning called a Gaussian process (GP) [18]. A GP is an extension of the multivariate Gaussian distribution, and it can be thought of as a nonparametric function of its input $\boldsymbol{x}$, with the distinction that, for any given $\boldsymbol{x}$, it returns a Gaussian distribution rather than a crisp number. As such, it is completely defined by a mean function and covariance function, defining the mean and (co)variance of the output distribution for any given input. An equivalent way of looking at it is that it is a distribution over functions; in a loose sense, it is a probability distribution where the random variable is a function rather than a scalar or a finite vector. GPs are especially well suited to emulator-based uncertainty analysis, because the GP accounts for its own uncertainty in its fit to the training data (since it is a probabilistic model). This uncertainty is passed on to the estimates of sensitivity indices, giving a full account of the estimation uncertainty in all stages.

To fit a GP to a given model, a Bayesian approach is used, whereby a prior mean function and covariance function are defined based on assumptions about the model and subsequently conditioned on a set of training data consisting of n input–output pairs $\boldsymbol{y} = \{f(\boldsymbol{x}_1), f(\boldsymbol{x}_2), \ldots, f(\boldsymbol{x}_n)\}$ (assuming that there is no measurement noise, as would be expected in a deterministic computer model). The prior mean is defined as a least-squares regression fit through the training data:

$$E\{f(\boldsymbol{x})|\boldsymbol{\beta}\} = \mathbf{h}(\boldsymbol{x})^T\boldsymbol{\beta} \tag{1}$$

where $\mathbf{h}(\boldsymbol{x})^T$ is a specified regression function of $\boldsymbol{x}$, and $\boldsymbol{\beta}$ is the corresponding vector of coefficients. The expectation is conditional on $\boldsymbol{\beta}$, because $\boldsymbol{\beta}$ is treated as unknown and is, itself, assigned a prior probability distribution: in this case, an improper prior (see, e.g., [19] for further information). For simplicity, $\mathbf{h}(\boldsymbol{x})^T$ was chosen to be $(1, \boldsymbol{x}^T)$, representing linear regression, although this can be extended to higher polynomial fits if there is some reason to suspect such a relationship. The covariance between output points is assumed to be

$$\operatorname{cov}\{f(\boldsymbol{x}), f(\boldsymbol{x}')|\sigma^2, B\} = \sigma^2 c(\boldsymbol{x}, \boldsymbol{x}') \tag{2}$$

where σ^2 is a scaling factor, and B is a diagonal matrix of length scales representing the smoothness of the output with respect to the individual input parameters. The specification of smoothness is the key to GP ability to reduce computational expense, since information from a data point (input) will allow inferences on the behavior of the function on neighboring points. The covariance function used here is a squared-exponential function of the form

$$c(\boldsymbol{x}, \boldsymbol{x}') = \exp\{-(\boldsymbol{x} - \boldsymbol{x}')^T B(\boldsymbol{x} - \boldsymbol{x}')\} \tag{3}$$

The posterior distribution is then found by conditioning the prior distribution on the training data $\mathbf{y}$, assigning weak priors to the hyperparameters σ^2 and $\boldsymbol{\beta}$, and then integrating them out (also known as marginalizing over them). This results in a Student's t process, conditional on B and the training data (for more details on the before posterior analysis, see [20]):

$$[f(\boldsymbol{x})|B, \mathbf{y}] \sim t_{n-q}\{m^*(\boldsymbol{x}), \hat{\sigma}^2 c^*(\boldsymbol{x}, \boldsymbol{x}')\} \tag{4}$$

where

$$m^*(\boldsymbol{x}) = \mathbf{h}(\boldsymbol{x})^T\hat{\boldsymbol{\beta}} + \mathbf{t}(\boldsymbol{x})^T A^{-1}(\boldsymbol{y} - H\hat{\boldsymbol{\beta}}) \tag{5}$$

$$\begin{aligned} c^*(\boldsymbol{x}, \boldsymbol{x}') = c(\boldsymbol{x}, \boldsymbol{x}') - \mathbf{t}(\boldsymbol{x})^T A^{-1}\mathbf{t}(\boldsymbol{x}') + [\mathbf{h}(\boldsymbol{x})^T \\ - \mathbf{t}(\boldsymbol{x})^T A^{-1}H](H^T A^{-1}H)[\mathbf{h}(\boldsymbol{x}')^T - \mathbf{t}(\boldsymbol{x}')^T A^{-1}H]^T \end{aligned} \tag{6}$$

$$\mathbf{t}(\boldsymbol{x})^T = [c(\boldsymbol{x}, \boldsymbol{x}_1), \ldots, c(\boldsymbol{x}, \boldsymbol{x}_n)]$$

$$H^T = [\mathbf{h}(\boldsymbol{x}_1), \ldots, \mathbf{h}(\boldsymbol{x}_n)]$$

$$A = \begin{pmatrix} 1 & c(\boldsymbol{x}_1, \boldsymbol{x}_2) & \ldots & c(\boldsymbol{x}_1, \boldsymbol{x}_n) \\ c(\boldsymbol{x}_2, \boldsymbol{x}_1) & 1 & & \vdots \\ \vdots & & \ddots & \\ c(\boldsymbol{x}_n, \boldsymbol{x}_1) & \cdots & & 1 \end{pmatrix}$$

$$\hat{\boldsymbol{\beta}} = (H^T A^{-1} H)^{-1} H^T A^{-1} \boldsymbol{y}$$

$$\sigma^2 = \frac{\boldsymbol{y}^T \{A^{-1} - A^{-1} H (H^T A^{-1} H)^{-1} H^T A^{-1}\} \boldsymbol{y}}{(n - d - 3)}$$

It is now possible, for any input point, to calculate the mean and variance of the emulator output using Eqs. (5) and (6), respectively (although the GP will not be used in this context here). Note that the determination of the emulator in Eq. (4) is basically an exercise in machine learning and, as such, its quality is critically dependent on the number and distribution of training data points in the input space and the values of the hyperparameters. The expressions for $\hat{\boldsymbol{\beta}}$ and $\hat{\sigma}^2$ result from the marginalization process and can be shown to be somewhat equivalent to least-squares estimates. The diagonal matrix of roughness parameters B cannot generally be integrated out analytically, and hence is evaluated using maximum a priori estimation (see, e.g., [21] for an explanation); this calculation typically represents the most computationally intensive part of the process.

B. Inference for Uncertainty/Sensitivity Analysis

Having established the emulator, a number of quantities of interest can be calculated that yield information about uncertainty and sensitivity of the model output. At the most basic level, the mean and variance of the output can be evaluated. Main effects show the response of the output with respect to variation of an individual input, giving a visual idea of linearity and sensitivity. Additionally, the effect of interactions between variables can be analyzed, which creates output uncertainty above and beyond the variation of those variables individually.

One can infer posterior mean values for main effects and interactions by simply substituting our posterior mean into the definition of the main effect, which is defined as the expected value of the output, conditional on some set p of input parameters:

$$E(Y|\boldsymbol{x}_p) = \int_{\chi_{-p}} f(\boldsymbol{x}) p_{-p|p}(\boldsymbol{x}_{-p}|\boldsymbol{x}_p)\, \mathrm{d}\boldsymbol{x}_{-p} \tag{7}$$

where the subscripts p and $-p$ denote the subset p and the complement of p, respectively, and χ_{-p} represents the range of input space in all dimensions except p. On substitution of Eq. (5) into Eq. (7) in place of $f(\boldsymbol{x})$, this yields

$$E^*\{E(Y|\boldsymbol{x}_p)\} = \mathbf{r}_p(\boldsymbol{x}_p)^T \hat{\boldsymbol{\beta}} + \mathbf{m}_p(\boldsymbol{x}_p)^T \mathbf{e} \tag{8}$$

where

$$\mathbf{r}_p(\boldsymbol{x}_p) = \int_{\chi_{-p}} \mathbf{h}(\boldsymbol{x}) p_{-p|p}(\boldsymbol{x}_{-p}|\boldsymbol{x}_p)\, \mathrm{d}\boldsymbol{x}_{-p} \tag{9}$$

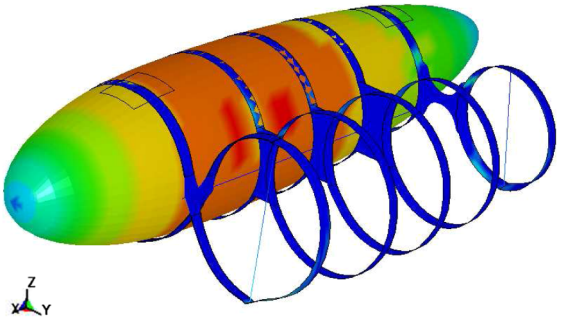

Fig. 5 Typical stress distribution of airship (one balloon removed for clarity).

$$\mathbf{m}_p(\boldsymbol{x}_p) = \int_{\chi_{-p}} \mathbf{t}(\boldsymbol{x}) p_{-p|p}(\boldsymbol{x}_{-p}|\boldsymbol{x}_p)\, \mathrm{d}\boldsymbol{x}_{-p} \qquad \mathbf{e} = A^{-1}(\boldsymbol{y} - H\hat{\boldsymbol{\beta}}) \tag{10}$$

Note that, when p is the null set, Eq. (8) yields the posterior mean of Y.

Additionally, Soboĺ sensitivity indices, which divide the variance of the output into portions that are attributed to each input and any interactions between them, can be calculated and represented in pie charts [15]. The main effect index (MEI) of an input variable i is represented as the variance of the output conditioned on that input:

$$V_i = \mathrm{var}\{E(Y|x_i)\} \tag{11}$$

This can be standardized by dividing by var(Y). Higher-order interactions can be examined by conditioning on sets of inputs. The posterior mean of these indices can be evaluated in a similar way to the main effect: full details are found in [20].

The tools detailed previously allow for uncertainty analysis of models with a substantial number of inputs, even if the run time of the model is prohibitively large for conventional MC techniques. It is worth emphasizing that, once the emulator is fitted, there is no need for further runs of the model or the emulator; the GP is chosen for its closed-form structure that allows fully analytical integration.

V. Results and Discussion

A. Dry Model

A two-dimensional parameter space was investigated, varying material temperature between −50 to +50°C (using the relationships illustrated in Fig. 2) and varying helium pressure. This second variable (in reality, the difference between internal and external pressure) was considered between 2 and 5 kPa. This was considered to be a plausible variation of pressure given a particular mission objective or a malfunctioning regulator valve.

The motor loading of the structure was considered to be an additional uncertainty, since in the event of a control system failure, the motors could conceivably be orientated in any direction. It is of course desirable that the structure be able to withstand this eventuality, however unlikely it might be. Since the consideration of eight additional motor angles would greatly increase the computing time required for the analysis, a separate static analysis was run with nominal temperature and pressure conditions for the motor loading conditions to find the most severe deformation, and this condition

Table 1 Mean and standard deviation of final-state stress over entire parameter space

Model region	Mean stress, MPa	Standard deviation, MPa	Standard deviation/stress, %
Balloon 1	14.8	1.13	7.6
Balloon 2	15.0	2.83	18.9
Belts	9.11	3.31	36
Frame	10.0	3.14	31.4
All	15.3	2.65	17.3

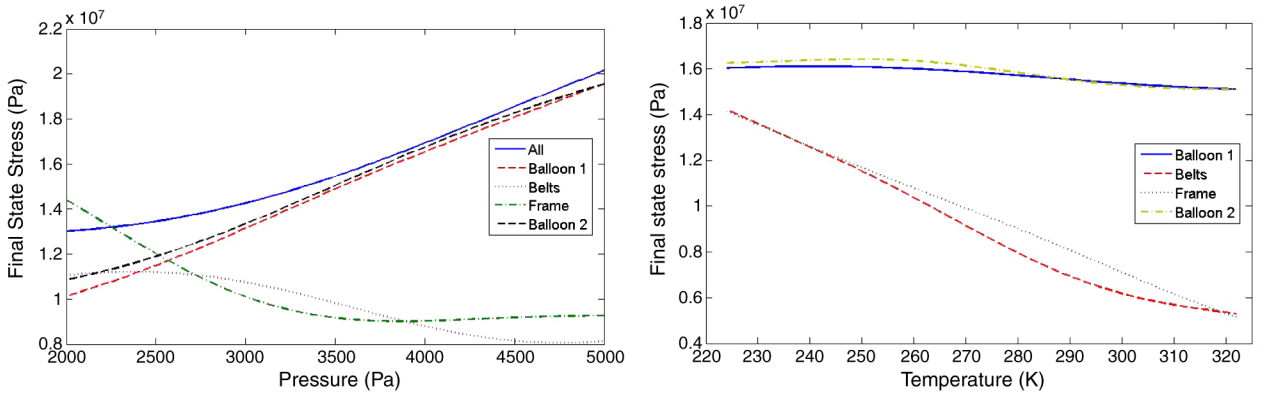

Fig. 6 Main effect plots for helium pressure (left) and temperature (right).

(representing a twisting of the frame) was used in the subsequent analysis.

Over the two-dimensional parameter space investigated, 15 training simulations were run by creating a space-filling design of experiments for each loading case. This sampling approach uses a constrained randomized method known as Latin hypercube sampling, based on a Latin square (see, e.g., [22] for further details). The design is further improved by maximizing the minimum distance between any two sample points (known as the maximin distance). The result is a design that is suitable for training nonparametric emulators such as the GP. The output of interest was the maximum stress in the structure, since this would indicate a possible failure. As such, maximum stress was extracted from each run from both the envelope and the composite frame. The stress value was taken from the final time step, since this represented the most stable state of the model after oscillations due to ramped loading were reduced to a minimum.

For each run, the maximum stress was collected at the final time step, as well as the maximum stress for any time step, for different parts of the model. The model was divided into the two balloons, the composite frame, and the belts. Of the 15 runs performed, two (corresponding to low frame stiffness) resulted in numerical failure about halfway through the simulation. This is typical of an uncertainty analysis of a complex nonlinear model; it is very difficult to construct a model that is stable over a wide input parameter space. Despite this, the 13 runs were still sufficient to conduct the analysis. For illustration, a typical final-state stress plot is shown in Fig. 5.

The overall uncertainty values are listed in Table 1. What is apparent from these values is that the uncertainty in the outputs investigated in the model is substantial, immediately justifying the use of uncertainty analysis techniques. This is to be expected, since an airship operates in a wide range of environmental conditions. In particular, the standard deviation of the frame stress is nearly one-third of the mean, a significant output uncertainty. Of course, stresses lower than the mean are not critical, but it is clear that taking mean temperature and pressure values would underestimate potential stress by a large extent. GP emulator uncertainty $\text{var}^*\{E(Y)\}$ for all outputs was found to be small, such that the posterior standard deviation of the mean was 100 kPa at most. This indicates that the GP can interpolate to unknown simulation points with a high level of confidence; in other words, the emulator is working well. If the emulator accurately mimics the behavior of the model, then the sensitivity analysis data are also of a high fidelity. Note that $\text{var}^*\{E(Y)\}$ is distinct from $E^*[\text{var}(Y)]$, which is the posterior estimate of the variance of the model output, presented in Table 1.

The main effect plots for the two inputs examined are presented in Fig. 6 to gain a more detailed insight into the influences of these parameters on the stress in various parts of the model. It should be remembered that these lines represent mean main effect values averaged over variations in the other parameter, i.e., the expected value of the output with respect to one parameter if we were to suddenly know the true value of the other parameter. This is in contrast with a one-at-a-time sensitivity analysis that examines the effect of varying one parameter without considering the effects of others. Examining the pressure plot first, the strongly linear relationship of stress and pressure is evident in the nearly straight lines representing both the balloons. The small differences between the two balloons are due to the asymmetry of the frame; loading conditions are not exactly the same for both balloons. A less obvious relationship is that of the frame stress and pressure. The fact that frame stress decreases with pressure suggests that, when the balloons are under greater tension due to pressure, they are impeding distortion in the frame from motor loading. This relationship of pressure and frame stress supports the hypothesis of the authors that a structural analysis of the frame without consideration of the balloon is inaccurate, since it plays an important part in the rigidity of the structure.

Regarding the main effects of temperature, it is apparent that the stress in the balloons is not strongly dependent on this parameter. The stress varies little between 16 and 17 MPa. Conversely, the stress of the frame is highly dependent on temperature. This is perhaps

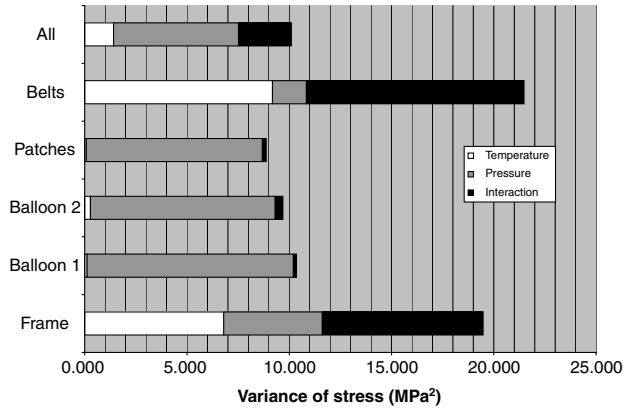

Fig. 7 Nonstandardized main effect indices and interactions for various model regions.

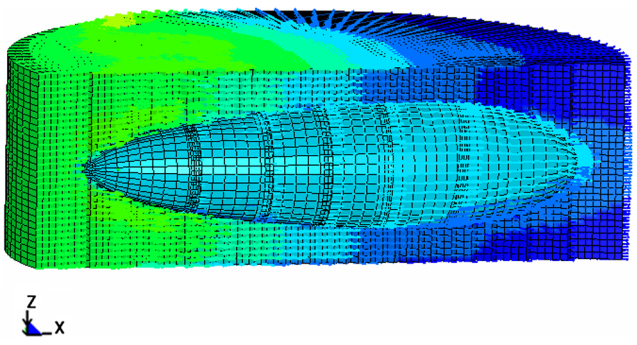

Fig. 8 Velocity vector plots of gust impact at $\mu = 0°$.

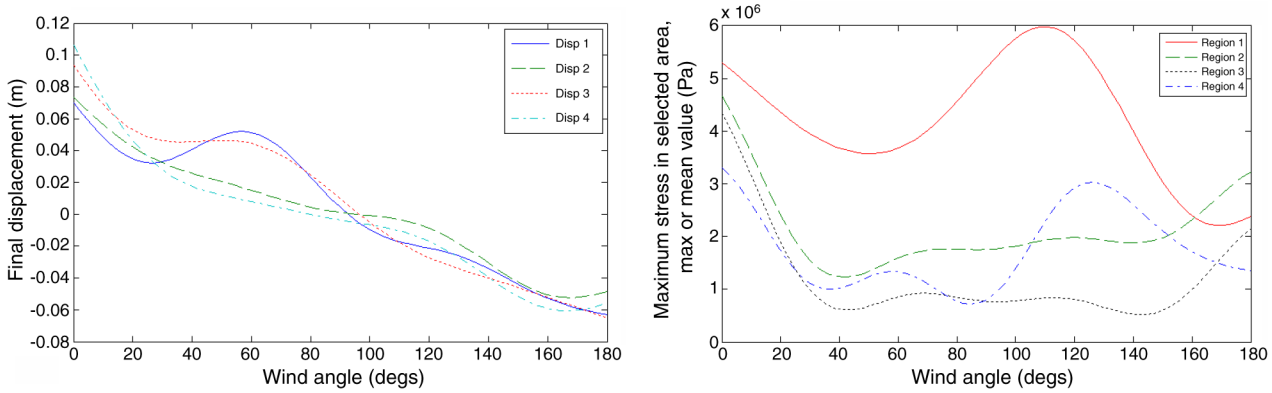

Fig. 9 Posterior means of displacements 1–4 (left), and posterior means of stress in regions 1–4 (right).

contrary to initial intuition, since the material properties of the frame vary little with temperature, while those of the envelope vary to a large extent. This is, however, evidence of the interactions at work in the model: loads are transferred between the frame and the balloons, so that a deformation in one part can cause a high stress increase in another part of the model.

A further result of the sensitivity analysis is shown in Fig. 7. The nonstandardized MEIs [see Eq. (11)] are summed for each model output, along with the output variance. This allows a comparison of the variance of stress in various parts of the model and the extent to which each of the two input parameters, or the interaction between them, is responsible for causing uncertainty in the output. As would be expected, the great majority of uncertainty in the balloon stress is due to the uncertainty in pressure. In the frame, temperature has a greater influence, but there are also significant interactions with the variation in pressure caused by the extra rigidity in the structure at higher pressures. Note that these trends can also be qualitatively observed from the plots of main effects, but the MEIs quantify the sensitivity of the output to each parameter to give a precise measurement. The main effect plots are still required, however, to see the exact relationship between an output and the variation in an input. Between the plots and the sensitivity indices, a very detailed picture of the model response can be built up.

Examination of the maximum stress values collected over all time steps in the model shows that they are up to 50% higher than the final time step stress in some cases. This is evidence of the higher stresses caused by initial fluctuations in the model, a drawback of using a dynamic analysis; yet, it is unavoidable due to the particular loading and constraint conditions of an airship.

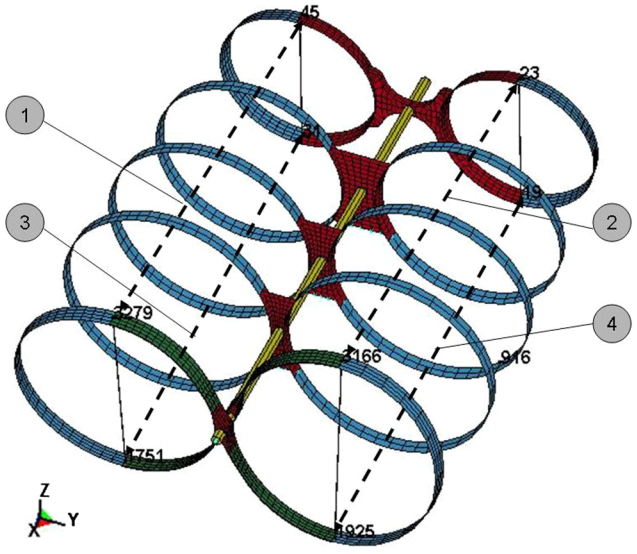

Fig. 10 Illustration of displacement measurements 1–4.

B. Wet Model

Figure 8 illustrates a velocity plot of the airflow around the airship hull. Examining the results from the wet model (Fig. 9) shows the main effects of final displacement between opposite propellers in the x direction of the model; see Fig. 10 (being a measure of the deformation of the structure, and thus degradation of the control system). Extracting a meaningful quantity from this model is not trivial, because the impact of the gust causes structural oscillations, and all displacement and stress values are a function of time. The variation in displacement is reasonably linear and quite small. This is attributed to the rigidity of the structure caused by tension in the balloons. The displacement is increasingly negative as the gust is angled more toward the front of the airship: likely because the balloon is pushed toward the rear of the ship, causing the structure to contract slightly.

Other outputs of the model are less well behaved. A significant difficulty with this model is that a small change in gust angle can drastically change the output of the model. Figure 9 shows the variation of stress with gust angle for four chosen regions in the model. Each of these regions represents an area of observed stress concentration in the frame (and thus a potential point of failure). The response of stress is shown to be highly nonlinear in relation to the gust angle. This does cause some problems, since a rough response requires a higher density of training data. An investigation of this (Fig. 11) uses leave-one-out cross validation (see, e.g., [15] for further explanation) to test the accuracy of the emulator for the stress in region 2. The emulator is constructed several times, each time leaving out one of the training data points. The mean and variance at each point is then noted. The results show that the variance of the emulator is large due to the combination of a rough response and an insufficient density of training data; however, all data are within the prediction. This suggests that a higher resolution of output data is necessary to investigate more accurately the true response of the model, but that the emulator is at least quantifying its own uncertainty

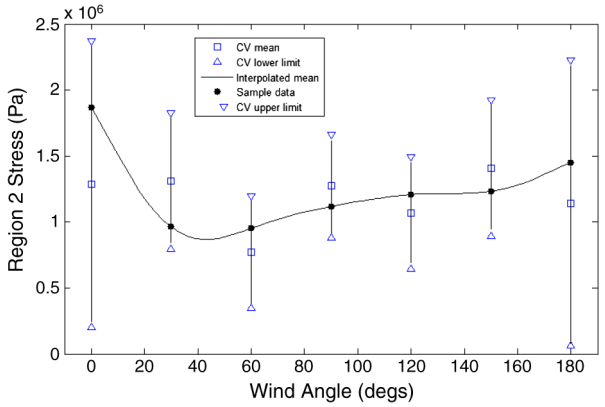

Fig. 11 Cross validation (CV) of region 2 stress emulator with 95% confidence limits.

correctly. Therefore, the results in Fig. 9 are in need of refinement but provide an insight into the problems that can occur in drawing conclusions from a very nonlinear model.

Finally, it should be noted that, in a model such as the one presented previously, the number of uncertainties can be extended almost without limit. Loading uncertainties such as wind pressure distribution, velocity, air density, and viscosity are but a few of the parameters that could vary due to environmental conditions or natural variation. Considering all these uncertainties in such a model is currently impractical, but it is worth remembering that considering only a small set of the model uncertainties can only result in an underestimate of the true output uncertainty.

VI. Conclusions

Typical FE models of an airship have been developed, and it was found that output uncertainty is significant, particularly when a low degree of aerodynamic loading is introduced. The GP emulator has been shown to be a powerful tool to investigate the magnitude of uncertainty in such models and, combined with sensitivity analysis data, can identify parameters that could reduce model uncertainty if they were known to a greater degree of accuracy. It is clear, however, that in highly nonlinear responses, a higher density of training data is required if meaningful conclusions are to be drawn from emulators such as the GP. Nevertheless, the GP acknowledges its own uncertainty in emulating the response of the model, and so when a poor emulator fit occurs, it can be easily identified. The overall benefit of emulator-based uncertainty analysis compared with MC methods is a substantial computational savings, which can be very significant in the case of a large computer simulation. The specific results gained from the airship show that uncertainty and sensitivity analyses are very important tools, given that computer models are used extensively in design, since an acknowledgement of the uncertainty in the model allows more informed decisions to be made about a particular design. Furthermore, sensitivity analysis allows a modeler to gain a deeper understanding of the interactions at work in a model by examining how variation in certain parameters affects various model outputs. Further work is required in the airship design presented here to test material uncertainty in the other candidate membrane materials.

Acknowledgments

The activity presented in this paper is part of the project entitled, "Innovative Solutions for Control Systems, Electric Plant, Materials and Technologies for a Non-Conventional Remotely-Piloted Aircraft," funded by the Piedmont Region of Italy. The authors would like to thank Ove Arup for the use of LS-Dyna.

References

[1] Liao, L., and Pasternak, I., "A Review of Airship Structural Research and Development," *Progress in Aerospace Sciences*, Vol. 45, Nos. 4–5, 2009, pp. 83–96. doi:10.1016/j.paerosci.2009.03.001

[2] Cappadona, A., Lecca, R., Vazzola, M., Gili, P., Farina, P., and Surace, C., "Innovative Unmanned Airship Structural Analysis: Dual-Hull and Exoskeletal Configurations," *Journal of Physics: Conference Series*, Vol. 181, No. 1, 2009, Paper 012097. doi:10.1088/1742-6596/181/1/012097

[3] Battipede, M., Lando, M., and Gili, P. A., "Peculiar Performance of a New Lighter-Than-Air Platform for Monitoring," AIAA 4th Aviation Technology, Integration, and Operations Forum, AIAA Paper 2004-6448, 2004.

[4] Battipede, M. P. G., Gili, P. A., and Lando, M., "Control Allocation System for an Innovative Remotely-Piloted Airship," AIAA Atmospheric Flight Mechanics Conference, Providence, RI, AIAA Paper 2004-4823, 2004.

[5] Battipede, M. P. G., Gili, P. A., Lando, M., and Massotti, L., "Flight Simulator for the Control Law Design of an Innovative Remotely-Piloted Airship," AIAA Modeling and Simulation Technologies Conference, Providence, RI, AIAA Paper 2004-4916, 2004.

[6] Cappadona, A., "Analisi Strutturale su Dirigible Non Convenzionale a Controllo Remoto: Configurazione Esoscheletro," Facoltà di Ingegneria, Politecnico di Torino, Torino, Italy, 2008.

[7] Lecca, R., "Analisi Strutturale su Dirigible Non Convenzionale a Controllo Remoto: Configurazione Bifuso," Facoltà di Ingegneria, Politecnico di Torino, Torino, Italy, 2008.

[8] *Polymer Matrix Composites Materials Properties*, Vol. 2, U.S. Dept. of Defense, Washington, D.C., 2002, Chap. 4.2.17.

[9] Bessert, N., and Frederich, O., "Nonlinear Airship Aeroelasticity," *Journal of Fluids and Structures*, Vol. 21, No. 8, 2005, pp. 731–742. doi:10.1016/j.jfluidstructs.2005.09.005

[10] Liu, J., Lu, C., and Xue, L., "Investigation of Airship Aeroelasticity Using Fluid–Structure Interaction," *Journal of hydrodynamics*, Vol. 20, No. 2, 2008, p. 164–171. doi:10.1016/S1001-6058(08)60042-6

[11] Li, Y., Nahon, M., and Sharf, I., "Dynamics Modelling and Simulation of Flexible Airships," *AIAA Journal*, Vol. 47, No. 3, 2009, pp. 592–605. doi:10.2514/1.37455

[12] "Airworthiness Code," *Certification Specifications for Normal, Utility, Aerobatic and Commuter Category Aeroplanes CS23*, European Aviation Safety Agency, Koeln, Germany, 2009.

[13] Donea, J. H. A., Ponthot, J.-Ph., and Rodriguez-Ferran, A., "Arbitrary Lagrangian–Eulerian Methods," *Encyclopedia of Computational Mechanics* [online], edited by E. Stein, de Borst, R., and Hughes, J. R. T., Wiley, New York, 2004, Chap. 14.

[14] Hallquist, J. O., "LS-Dyna Theory Manual," Livermore Software Technology Corp., Livermore, CA, 2006, Chap. 26.3.

[15] Saltelli, A., Chan, K., and Scott, E. M., *Sensitivity Analysis*, Wiley Series in Probability and Statistics, Wiley, New York, 2000.

[16] George, J. K., and Richard, M. S., "On Measuring Uncertainty and Uncertainty-Based Information: Recent Developments," *Annals of Mathematics and Artificial Intelligence*, Vol. 32, Nos. 1–4, 2001, pp. 5–33. doi:10.1023/A:1016784627561

[17] Oakley, J. E., and O'Hagan, A., "Probabilistic Sensitivity Analysis of Complex Models: A Bayesian Approach," *Journal of the Royal Statistical Society Series B (Methodological)*, Vol. 66, No. 3, 2004, pp. 751–769. doi:10.1111/j.1467-9868.2004.05304.x

[18] Sacks, J., Welch, W. J., Mitchell, T. J., and Wynn, H. P., "Design and Analysis of Computer Experiments," *Statistical Science*, Vol. 4, No. 4, 1989, pp. 409–435. doi:10.1214/ss/1177012413

[19] Gelman, A., Carlin, J. B., Stern, H. S., and Rubin, D. B., *Bayesian Data Analysis*, 2nd ed., CRC Press, Boca Raton, FL, 2004, pp. 61–65.

[20] Becker, W., Rowson, J., Oakley, J., Yoxall, A., Manson, G., and Worden, K., "Bayesian Sensitivity Analysis of a Nonlinear Finite Element Model," *Mechanical Systems and Signal Processing* (submitted for publication).

[21] Rasmussen, C. E., and Williams, C. K. I., "Gaussian Processes for Machine Learning," *Adaptive Computation and Machine Learning*, Massachusetts Inst. of Technology, Cambridge, MA, 2006, Chap. 5.4.1.

[22] Fang, K., Li, R., and Sudjianto, A., *Design and Modeling for Computer Experiments*, CRC Press, Boca Raton, FL, 2006, Chap. 2.